Investigation of barrier inhomogeneities in *I-V* and *C-V* characteristics of Ni/*n*-TiO$_2$/*p*-Si/Al heterostructure in wide temperature range

Arvind Kumar*, K.K. Sharma, Subhash Chand, Ashwani Kumar[1]

Department of Physics, National Institute of Technology, Hamirpur, H.P., 177005, India

A B S T R A C T

In this study, we report on the growth and electrical characterization of Ni/*n*-TiO$_2$/*p*-Si/Al heterojunction. A thin layer of TiO$_2$ was deposited on *p*-Si by pulsed layer deposition technique. Highly pure nickel and aluminum metals were deposited by thermal coating system to make the contacts to *n*-TiO$_2$ and *p*-Si, respectively. The pulsed laser ablation processed Ni/*n*-TiO$_2$/*p*-Si/Al heterojunction exhibits good rectifying properties over the wide range of temperature between 80 K and 300 K. The X-ray diffraction (XRD) investigations have confirmed the epitaxial growth of the TiO$_2$ films which are highly oriented nanocrystals with particle size of 43.3 nm. The optical energy band gap of TiO$_2$ thin films was studied using *UV-VIS* spectroscopy and Tauc plots, which comes out to be 3.20 eV. Atomic force microscopy study of the surface morphology reveals that the surface is reasonably smooth, homogeneous and the roughness is of nanometer order. The dominating current transport mechanisms through the heterojunction were investigated in forward and reverse bias current-voltage (*I-V*) measurements. The current transport mechanisms are strong functions of temperature and successfully explained using thermionic emission diffusion (TED) mechanism with Gaussian distributions of barrier heights. The dependence of barrier height on temperature and the non-linearity of activation energy plot have confirmed that barrier heights at *n*-TiO$_2$/*p*-Si interface follow the Gaussian distributions. The mean value of barrier height and standard deviation were found to be 0.79 eV and 0.10 V, respectively. The effective resistance of the heterojunction plays an important role in the *I-V* characteristics as well as in rectifying properties. The barrier heights as a function of temperature were also studied from reverse biased capacitance-voltage (*C-V*) characteristics. The discrepancy between the barrier heights calculated from *I-V* and *C-V* measurements has been attributed to the existence of barrier inhomogeneities and tunneling factor in the current transport mechanisms. The value of Richardson's constant found to be $1.5 \times 10^5 \, \text{Am}^{-2} \text{K}^{-2}$ which is of the order of known theoretical value of $3.2 \times 10^5 \, \text{Am}^{-2} \text{K}^{-2}$.

1. Introduction

Titanium dioxide (TiO$_2$) is a non-toxic *n*-type wide band gap semiconductor material with low production cost and high-temperature stability. TiO$_2$ crystallizes in three polymorphs namely rutile, anatase and brookite. Anatase is metastable phase that can be

---

* Corresponding author
  E-mail address: akpurinithmr@gmail.com (A. Kumar).
[1] Government College Bilaspur (H.P.) 174001, India.

synthesized only in the restricted range of growth conditions. Brookite phase is obtained only in extreme conditions during synthesis, while rutile phase is most common and thermodynamically most stable [1].

Metal-semiconductor contacts are most widely used for rectifying characteristics in the electronics industry [2,3]. Recently, researchers have worked to improve the electrical transport properties of Schottky barrier diodes (SBDs) by fabricating inorganic interfacial layers to form metal-semiconductor and metal-insulator-semiconductor diodes [4–8]. The *I-V* characteristics of SBDs show decrease in the barrier height while an increase in the ideality factor as the temperature decreases in accordance with thermionic emission theory [9,10]. The barrier height and the ideality factor are strongly temperature dependent parameters [11–13].

The presence of an interfacial layer between the metal top contact and semiconductor could modify the electric characteristics of the structure mainly by increasing the barrier height of the structure [3]. The TiO_2 films are extensively studied due to their interesting chemical, optical and electrical properties [14]. The main advantages of TiO_2 films are the low density of interface states and high dielectric constant [15–20]. The TiO_2 is a potential candidate with high thermal stability, large band gap, high refractive index and low leakage current as interfacial thin film used to improve the efficiency of electrical and optical devices [21–28]. The TiO_2 thin films have found numerous applications in electronic device applications [29]. The fabricated heterostructures considerably improve the electric characteristics of the devices [30]. In the recent years, there has been increasing interest in the study of the electrical properties of SBDs due to their excellent rectifying properties [3]. Moreover, the nanostructured materials significantly enhance heterojunction effects and junction's properties of the Schottky based sensors [31,32]. The electrical properties of SBDs depend especially on the series resistance of the device [33]. The *I-V* properties of these devices do not obey the ideal Schottky theory. The use of thermionic emission theory to obtain SBDs parameters, records a decrease of the zero-bias barrier height and an increase in ideality factor with decreasing temperature which leads to the non-linear behavior of activation energy plots [9]. The spatial barrier inhomogeneities were described mainly by Gaussian distribution function used to correlate the experimental data [10]. The current transport mechanism in SBDs obey the field emission and Gaussian distribution of barrier heights rather than other mechanisms [22]. There are evidences of the presence of compensating acceptor levels in the niobium doped TiO_2 films prepared by the sol-gel layer-by-layer technique and it was established that conduction mechanism is based on space charge limited current through deep levels with different energy position in the band gap [11]. The Ohmic-Schottky and Schottky-Schottky combination in metal-oxide-metal devices promotes the unipolar resistive switching whereas Ohmic-Ohmic combinations do not show the resistive switching behavior [34]. In the heterostructure $Pt/TiO_2/Ti$ for resistive switching, the Pt/TiO_2 corresponds to the blocking whereas TiO_2/Ti corresponds to the ohmic contacts [35]. Various techniques can be used to obtain TiO_2 thin films [36–38] but the pulsed laser deposition (PLD) technique allows one to obtain homogeneous thin films with high reproducibility [39]. In the present work, our aim is to grow single rutile phase TiO_2 thin film to fabricate the Ni/n-TiO_2/p-Si/Al heterojunction diode using PLD technique and to study the optical, structural properties as well as *I-V* and *C-V* characteristics in wide temperature range between 80 K and 300 K. The study of *C-V* characteristics at different frequencies has also been performed. Donor concentration N_D, built-in voltage V_{bi}, fermi energy E_f, effective density of states in the Si valance band N_C, depletion layer width W_D, interface states N_{SS}, maximum electric field E_m, image force barrier lowering, $\Delta\varphi_b$ parameters have also been obtained from *C-V* measurements.

2. Experimental procedure

The thin films of TiO_2 were grown on *p*-type (boron doped) single crystal silicon wafer with (100) surface orientation by pulsed laser ablation technique to fabricate Ni/n-TiO_2/p-Si/Al heterojunction diode. Prior to the fabrication process the Si wafer was sequentially cleaned with organic solvents C_2HCl_3, CH_3COCH_3 and CH_3OH and deionized water under constant ultrasonication for 10 min at each step. After organic cleaning, the silicon wafer was etched in a 40% HF solution to remove the native oxide layer then finally again rinsed with deionized water. Immediately after cleaning process, Si wafer was transferred into the deposition chamber. High purity (99.999%) aluminum metal was deposited under 3×10^{-6} mbar vacuum on the back side of the silicon wafer to form the ohmic contacts and then wafer was annealed for 1 h at 300 °C to achieve good ohmic behavior. The TiO_2 film was grown on the front side i.e. polished side of silicon wafer by pulsed laser deposition technique. Before TiO_2 thin film deposition, the silicon wafer was cleaned and etched in 40% HF solution for one minute to clean off native oxide layer formed on silicon surface. Picein coating was used to protect the back ohmic contact of aluminum metal.

Pure TiO_2 powder was thoroughly grinded in agate mortar and pressed in the form of circular pallets of 50 mm diameter by applying a pressure of 5–6 ton in hydraulic press. The TiO_2 pallets used for deposition were sintered at 1000 °C for 12 h. The KrF (248 nm) COHERENT COMPLEX PRO 205 F laser with repetition rate of 10 Hz at energy of 300 mJ was used to ablate the TiO_2 target. The chamber was evacuated to a base pressure of 3×10^{-6} mbar before the commencement of deposition. The oxygen partial pressure of 7×10^{-3} mbar was maintained during the deposition and the substrate to target distance was kept 5 cm. Finally, nickel metal was thermally evaporated from the tungsten filament into TiO_2 film surface through masks with circular holes of 1 mm diameter under 3×10^{-6} mbar vacuum to get the metal contacts. No energy barrier formation was detected between TiO_2 and vacuum-deposited metal contacts [23,42]. The schematic diagram of the device and measurement system is shown in Fig. 1. For electrical characterization, the forward and reverse bias *I-V* measurements were carried out in the temperature range of 80 K–300 K using a programmable Keithley 2400 source-meter. The Lakeshore 331 auto-tuning temperature controller with sensitivity better than ± 1 K and a close cycle helium refrigeration system was used to monitor the sample temperature. The electrical measurements were performed by making use of microcomputer through an IEEE-488 interface card. Wayne Kerr 6520A, precision impedance analyzer was employed to study the *C-V* measurements. X ray diffraction pattern of thin films were obtained by using Panalytical Xpert Pro diffractometer. Non-contact mode AFM images were performed by SPM 5500 (Agilent) using closed loop scanner with non-contact low frequency silicon cantilever (force constant: 21–98 N/m). The optical measurements were performed by using Perkin
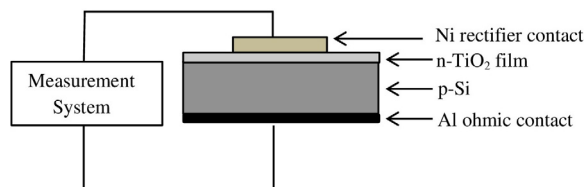
Fig. 1. Schematic diagram of Ni/*n*-TiO$_2$/*p*-Si/Al heterojunction.

Elmer Lambda-750 spectrophotometer.

3. Results and discussion

3.1. XRD studies

The XRD pattern of the prepared TiO$_2$ layer is shown in Fig. 2. The structural investigations confirmed the existence of TiO$_2$ thin film on *p*-Si wafer with low intensity peaks at an angle (2θ) 27.21° and 44.65° corresponding to Bragg reflections (110) and (210), respectively and no impurity phases were observed. These peaks correspond to rutile phase of TiO$_2$, which are in good agreement with the JCPDS Card No. 03-065-0191. The strong peaks at an angle (2θ) 32.99° and 69.13° corresponds to the Si(002) and Si(004) reflections. The grown TiO$_2$ thin film exhibit crystalline behavior with (210) as preferred orientation [12,13].

The crystallite size D of the TiO$_2$ film was determined using Scherrer equation [43]:

$$D = \frac{K\lambda}{\beta \cos \theta}$$

(1)

where, K is constant taken to be 0.94, β is the full width at half maximum of the selected diffraction peak at 2θ, θ is the Bragg's diffraction angle and λ is the wavelength of the incident X-rays which is 1.54 Å. The (210) peak analysis has confirmed 43.3 nm average grain size of TiO$_2$ film. The grain size depends upon the synthesis conditions, the comparable grain size of 43.3 nm was found in the literature [44].

3.2. Optical band gap study

The optical measurements were performed in the range between 250 nm and 800 nm for the TiO$_2$ thin film deposited on quartz substrate using *UV/VIS* spectrophotometer to obtain the transmission spectrum as shown in Fig. 3. The TiO$_2$ thin film exhibits sharp absorption edge within ultraviolet region which corresponds to optical energy band gap (E$_g$). The value of E$_g$ has been determined from the transmission measurements using the $(\alpha h\upsilon)^n$ versus energy plot, with

$$\alpha h\upsilon = A(h\upsilon - E_g)^n$$

(2)

where, α is the absorbance value, $h\upsilon$ is the incident photon energy and A is the optical absorption edge width parameter. In TiO$_2$, indirect allowed transitions dominate in the optical absorption edge for which the value of exponent, $n = 1/2$ [45,46]. The absorption coefficient in the indirect band gap semiconductor TiO$_2$ above the threshold of fundamental absorption can be determined
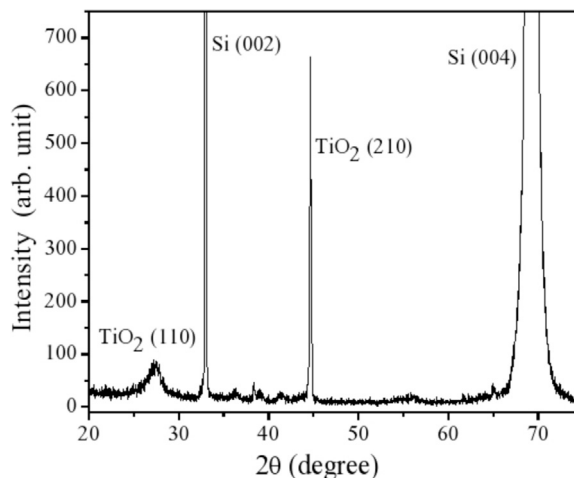

Fig. 2. X-ray diffraction spectra of TiO$_2$ film deposited on p-type silicon.

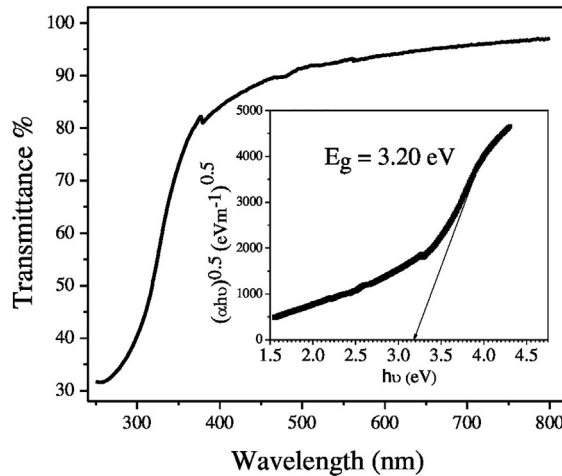**Fig. 3.** Optical transmittance spectra of TiO_2 thin films on quartz as a function of wavelength. The inset graph shows the plots of $(\alpha h\upsilon)^{1/2}$ versus photon energy ($h\upsilon$).

by using Tauc plot [47] shown in the inset of Fig. 3. The optical absorption edge which corresponds to the optical energy gap of TiO_2 film was obtained by extrapolating the value of $(\alpha h\upsilon)^{1/2}$ to $\alpha = 0$ in the sharp absorption edge region. This gives the band gap energy of TiO_2 equal to 3.20 eV, which is in good agreement as reported in literature [48]. The indirect bandgap of rutile TiO_2 is 3.0 eV [49]. The increased value of bandgap may be attributed to the nanostructure of the thin film. TiO_2 thin films on *p*-Si can be used for UV (Ultraviolet) detection due its natural n-type wide bandgap semiconductor nature [50].

3.3. AFM studies

Non-contact mode atomic force microscope (AFM) was brought in use to estimate the surface roughness of TiO_2 film over a $10 \times 10\,\mu m^2$ area. The AFM images (2D and 3D) showing the surface morphology of TiO_2 thin film on *p*-type silicon wafer are given in Fig. 4(a) and(b), respectively. These AFM images show reasonably smooth film with uniform grain distribution. These AFM images also show the growth of thin film with condensed columnar structures without visible pores and defects in the film. The TiO_2 films grown by PLD technique are found to possess homogeneous distribution of grains. The estimated roughness (Rq) of TiO_2 thin film was found to be 2.9 nm. These AFM studies confirm the formation of reasonably smooth and homogeneous TiO_2 films with surface roughness of nanometer order.

3.4. Current-voltage characteristics

Fig. 5 shows the semilog forward and reverse bias *I-V* characteristics of Ni/*n*-TiO_2/*p*-Si/Al heterojunction for the current applied perpendicular to the film surface with typical junction area 1 mm^2, which clearly demonstrates the asymmetry with respect to
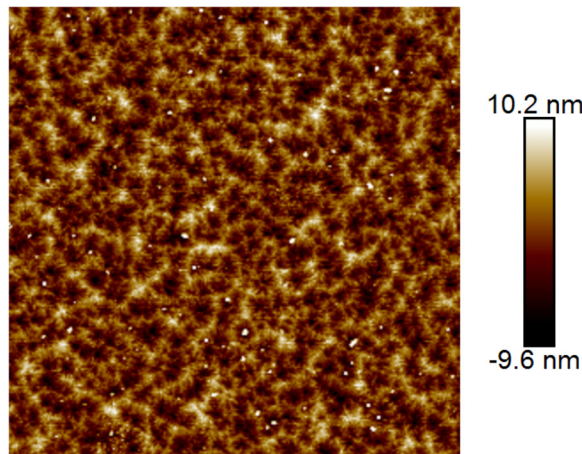

Fig. 4. a Atomic force microscopy 2D image of TiO_2 thin film on *p*-type silicon. b Atomic force microscopy 3D image of TiO_2 thin film on *p*-type silicon
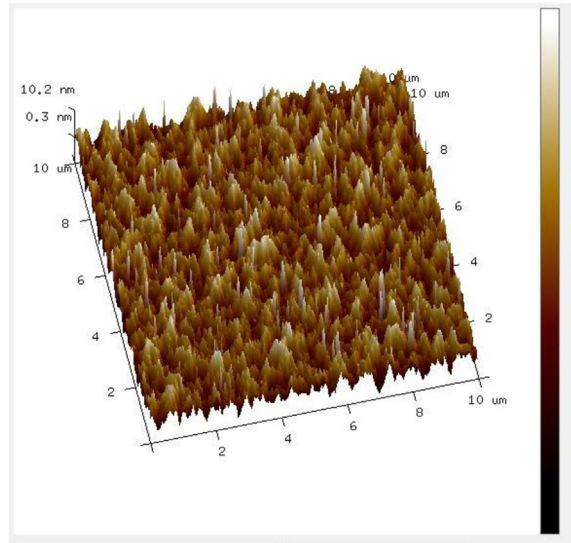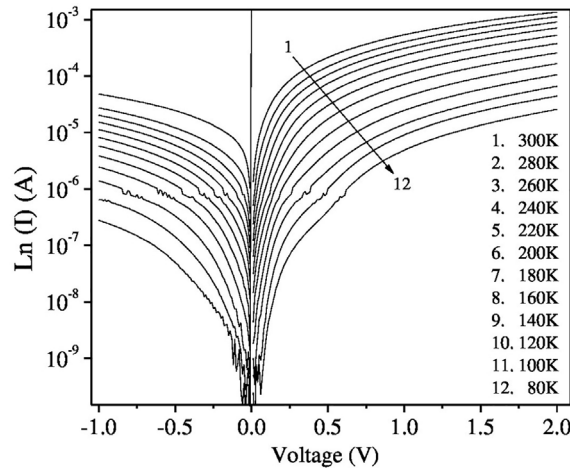
Fig. 4. (*continued*)

Fig. 5. Current-voltage characteristics of Ni/*n*-TiO$_2$/*p*-Si/Al heterojunction diodes at different temperatures.

forward and reverse bias, indicating good rectification over the wide range of temperature. There is exponential increase in the forward current with increase in the forward bias. The thermally generated minority carriers result in increase in the reverse saturation current with increase in the measuring temperature. At room temperature, the linear portion is limited to small bias voltages because of the low barrier prevailing at the interface of the heterojunction. As the temperature increases from 80 K to 300 K, the slopes of the *I-V* curves become steeper for the forward bias voltages. This behavior of the heterojunction makes it different from conventional diode, where the *I-V* characteristics are almost independent of temperature in the forward bias conditions. It was attributed to the fact that carriers are driven over the energy barrier at the interface with increasing temperature by the smaller applied bias voltages due to the Richardson's effect. Moreover, the curves are linear at low applied voltages and become non-linear at high forward voltages due to the existence of series resistance. The stable rectification without interference with resistive switching obtained for Ni/*n*-TiO$_2$/*p*-Si/Al heterostructure shows its satisfactory reliability for one diode one resistor electronic memory devices [51]. The current through the heterojunction at a forward bias is given by well-known thermionic mechanism:

$$I = I_S \exp\left(\frac{q(V - IR_S)}{\eta kT}\right)\left[1 - \exp\left(\frac{-q(V - IR_S)}{kT}\right)\right]$$

(3)

with

$$I_S = A_d A^{**} T^2 \exp\left(\frac{-q\varphi_{b0}}{kT}\right)$$

(4)

where I_S is the reverse saturation current, A_d is diode contact area, A^{**} is the effective Richardson constant which is 3.2×10^5
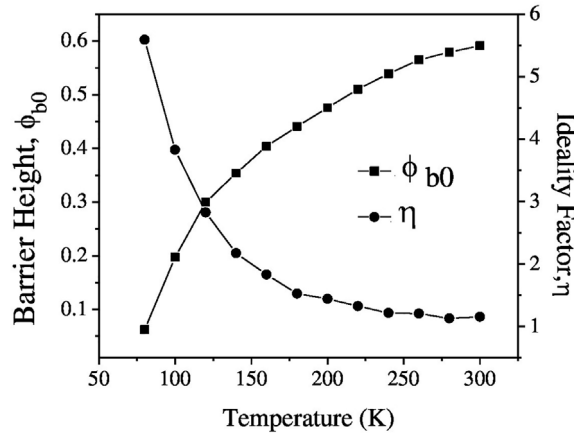
Fig. 6. Barrier height and ideality factor as a function of temperature for Ni/*n*-TiO$_2$/*p*-Si/Al heterojunction diode.

Am^{-2}K^{-2} for *p*-Si, T is the absolute temperature, k is the Boltzmann constant, q is the charge of electron, φ_{b0} is the zero-bias barrier height, η is a dimensionless ideality factor and IR_s is the voltage drop caused by series resistance R_s. The barrier height and ideality factor can be obtained from the forward biased part of the *I-V* curves through the relations:

$$\varphi_{b0} = \frac{k\,T}{q}\ln\left(\frac{AA^{**}T^2}{I_S}\right)$$
(5)

$$\eta = \frac{q}{kT}\frac{dV}{d(lnI)}$$
(6)

The intercept of the extrapolated ln(I)-V plot on the current axis provide the reverse saturation current, I_S. Fitting of *I-V* data in equation (3) has been done by bringing MATLAB program in use, taking I_S , η and R$_s$ as adjustable parameters. The φ_{b0} values are calculated from equation (4) while the slopes of the ln(I)-V plots in linear regions provide the values of ideality factor, η. Fig. 6 shows the variations of the φ_{b0} and η with the temperature. The barrier height increases while the ideality factor decreases with rise in the temperature. The values of φ_{b0} were found to be strongly temperature dependent and decreases from 0.59 eV to 0.062 eV on decreasing temperature from 300 K to 80 K. At low temperatures the current transport is dominated by the electrons which surmount the lower barriers and hence indicate the tunneling mechanism. These results are compatible with the observations reported for Al/*n*-TiO$_2$/*p*-Si heterojunction in the literature [10]. The extracted values of ideality factor are relatively small from room temperature to 180 K. Below this temperature the ideality factor initially increases marginally with decrease in temperature and then significantly below 160 K acquiring a value of 5.59 at 80 K. The large values of ideality factor show the deviation from thermionic emission theory in the current transport mechanism due to series resistance effect in Ni/*n*-TiO$_2$/*p*-Si/Al heterojunction. The observed variations in Fig. 6 are due to the inhomogeneity in thickness of grown TiO$_2$ thin film and non-uniformity of the interfacial charges [37].

Equation (4) can be rewritten as

$$\ln\left(\frac{I_S}{T^2}\right) = \ln(A_dA^{**}) - \frac{q\varphi_{b0}}{kT}$$
(7)

The equation provides the second way to calculate activation energy from the saturation current density values by plotting ln(I$_s$/T^2) versus 1/T for the heterojunction, which is called Richardson's plot and it should be a straight line. The slope and the intercept of this straight line give the values of barrier height φ_{b0} and Richardson constant A^{**} if diode contact area A_d is known. The ln(I$_s$/T^2) vs 1000/T profile as shown in Fig. 7 is found to be non-linear in the measured temperature range which depicts the temperature dependence of the barrier height and the ideality factor. The asymptotic fitting of the experimental data with a straight line is possible only at higher temperature. Richardson constant A^{**} is found to be 2.33 × 10^{-3} Am^{-2}K^{-2} and the mean activation energy 0.13 eV at higher temperatures. The obtained value of Richardson constant is affected by the lateral inhomogeneities and potential fluctuations of the barriers at the interface of the heterojunction so it is much lower than the theoretical known value of 3.2 × 10^5 Am^{-2}K^{-2} for *p*-Si [40]. These findings clearly indicate the deviation from pure thermionic emission mechanism and hence further investigations are required to understand the observed behavior.

3.5. Analysis of barrier height inhomogeneities

In spite of the discrepancy in the barrier height, ideality factor, Richardson's constant and their temperature dependence, the *I-V* characteristics can still be explained by equation (3) considering that barrier height inhomogeneities has a Gaussian distribution with mean barrier height $\overline{\varphi}_{b0}$ and standard deviation σ [41,52–54], which yields the following expression for the Gaussian distribution of barrier heights:
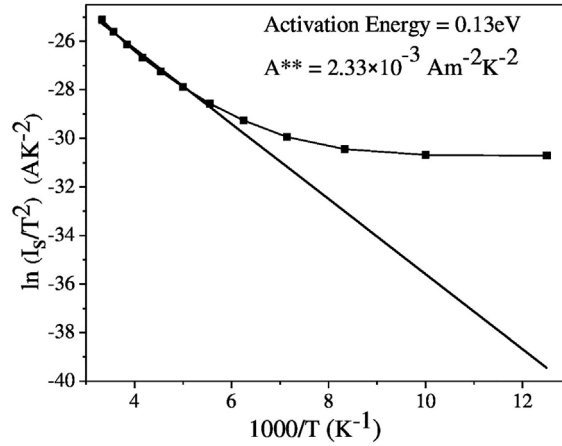
Fig. 7. The activation energy plot of Ni/n-TiO$_2$/p-Si/Al heterojunction diode.

$$\varphi_{ap} = \bar{\varphi}_{b0} - \frac{q\sigma^2}{2kT}$$

(8)

where φ_{ap}, σ, $\bar{\varphi}_{b0}$ stands for apparent zero-bias barrier height measured experimentally, standard deviation and mean barrier height respectively. The variations of φ_{b0} versus 1000/T as shown in Fig. 8 give the values of mean barrier height and the standard deviation for the Ni/n-TiO$_2$/p-Si/Al heterojunction. The intercept and slope of the straight line yields mean barrier height $\bar{\varphi}_{b0} = 0.79$ eV and standard deviation $\sigma = 0.10$ V, respectively. The standard deviation is the measure of the barrier inhomogeneity and provides the evidence of the presence of Gaussian distributions of barrier heights at interface of the n-TiO$_2$/p-Si heterojunction. The Gaussian distributions of barrier heights and potential fluctuations modify the transport mechanism in the heterojunction especially at low temperatures.

Using equations (7) and (8) the Richardson's plot gets modified as:

$$\ln\left(\frac{I_S}{T^2}\right) - \frac{q^2\sigma^2}{2k^2T^2} = \ln(A_d A^{**}) - \frac{q\bar{\varphi}_{b0}}{kT}$$

(9)

The modified activation energy $\ln\left(\frac{I_S}{T^2}\right) - \frac{q^2\sigma^2}{2k^2T^2}$ versus 1000/T plot along with the original activation energy is shown in Fig. 9. In accordance with equation (9) the modified Richardson's plot exhibits linearity over the whole temperature range corresponding to single activation energy. The slope and the intercept at the ordinate yield the mean barrier height $\bar{\varphi}_{b0}$ and the Richardson's constant A^{**}. The least squares linear fitting of the data gives the improved values of A^{**} and $\bar{\varphi}_{b0}$ as 1.5×10^5 Am^{-2}K^{-2} and 0.70 eV, respectively.

3.6. Capacitance-voltage characteristics

The depletion region formed at the interface of n-TiO$_2$/p-Si may be treated as a bias-dependent capacitor. The C-V measurements
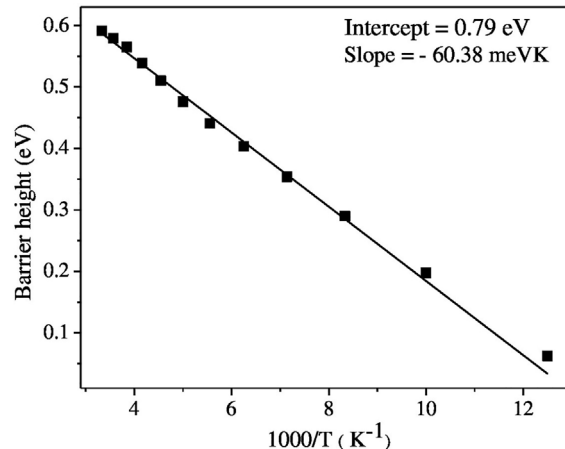

Fig. 8. The apparent barrier height φ_{ap} obtained from I-V measurements as a function of inverse temperature.
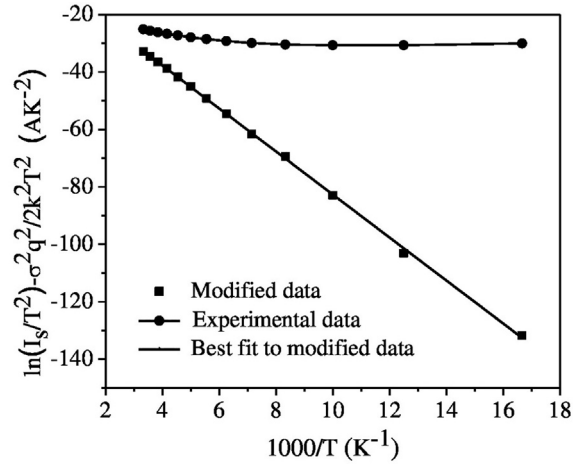
Fig. 9. Modified activation energy plots corresponding to the standard deviation σ = 0.10V.

are the important non-destructive method for obtaining the information on rectifying heterostructures. Fig. 10 shows the (C-V) characteristics of Ni/n-TiO$_2$/p-Si/Al heterojunction measured at room temperature with frequencies of 100 kHz, 500 kHz and 1 MHz using impedance analyzer (Wayne Kerr 6520A). The interface states influence the measured capacitance at low frequencies and series resistance effect is observed at high frequencies. Hence impact of the frequency of applied AC signal on the measured capacitance must be considered. Moreover, in Fig. 10 the saturation region (from 0 to -5V) depicts complete depletion of barrier height junction layer while the region from 0 to 1 V, reveals that the width of the depletion region decreases with the increase in the forward bias [55,56].

The measured C-V characteristics in the Mott-Schottky plots show the linear dependence at frequencies of 100 kHz, 500 kHz and 1 MHz with slope values of 4.18×10^{-13} m^2/(nF)^{2}V, 4.79×10^{-13} m^2/(nF)^{2}V and 5.85×10^{-13} m^2/(nF)^{2}V, respectively as shown in Fig. 11. The slopes increase with increase in frequency which is due to the electrically active surface states at the heterojunction interface and bulk traps within the depletion region [55,56]. The voltage and frequency dependence are the function of Schottky barrier, interface states and series resistance. To investigate the junction capacitance behavior of considered heterostructure, the reverse biased C-V measurements are also taken at different temperatures. The C-V characteristics of the heterostructure can be analyzed using the following relation [57,58]:

$$\frac{1}{C^2} = \frac{2(V_{bi} + V)}{q\varepsilon_S \varepsilon_0 A^2 N_D}$$

(10)

where, N_D represents the electron carrier concentration, ε_0 is the permittivity of free space, ε_s is the dielectric constant of semiconductor (Si), V_{bi} is built-in voltage.

Fig. 12 shows the reverse bias C^{-2} versus V characteristics of the heterostructure in the temperature range of 80 K–300 K at 1 MHz frequency. If it is fitted, the intercept of the line on voltage axis (i.e. $C^{-2} = 0$) gives the built-in voltage or diffusion potential, V_{bi} while
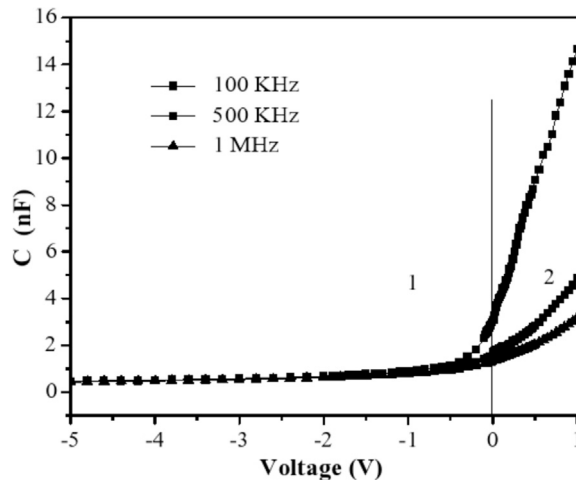

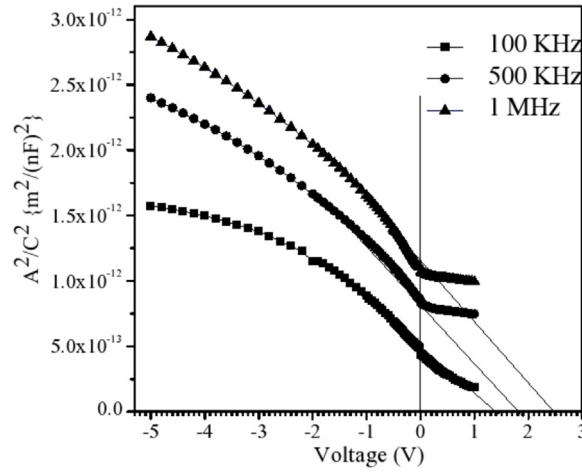Fig. 10. The C-V-f characteristics of the Ni/n-TiO$_2$/p-Si/Al heterojunction diode measured at room temperature.

Fig. 11. Mott-Schottky plots of the capacitance-voltage characteristics of the Ni/n-TiO$_2$/p-Si/Al heterojunction diode.
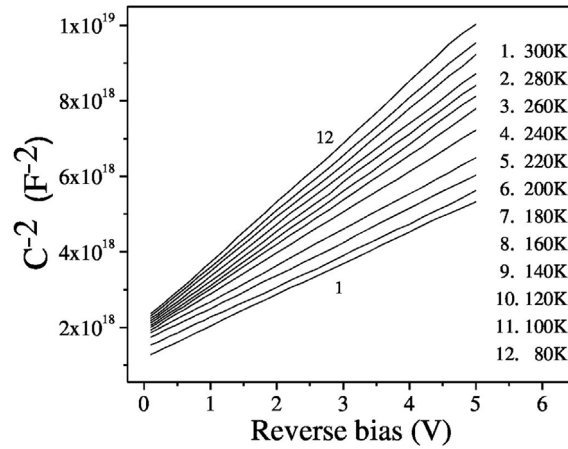

Fig. 12. The $1/C^2$ vs V characteristics of the Ni/n-TiO$_2$/p-Si/Al heterojunction diode at a frequency of 1 MHz at different temperatures.

from the slope of the profile the donor carrier concentration N_D was calculated. V_0 is the intercept of C^{-2} with the voltage axis and is related to V_{bi} as:

$$V_{bi} = V_0 + \frac{kT}{q} \tag{11}$$

The value of the barrier height can be obtained from C-V data using the relation [59].

$$\varphi_{b(C-V)} = V_{bi} + E_f - \Delta\varphi_b \tag{12}$$

where E_f is the energy difference between bulk Fermi level and the conduction band edge and is given by Ref. [60].

$$E_f = \frac{kT}{q} \ln \frac{N_C}{N_D} \tag{13}$$

with

$$N_C = 4.82 \times 10^{15} T^{3/2} \left(\frac{m_e^*}{m_0} \right)^{3/2}$$

where, m_e^* is the effective mass of electrons, m_0 is the rest mass of the electron and N_C is the effective density of states in the Si valance band. $\Delta\varphi_b$ is the image force barrier lowering and is given by Ref. [3].

$$\Delta\varphi_b = \left(\frac{qE_m}{4\pi\varepsilon_S\varepsilon_0} \right)^{1/2} \tag{14}$$

where E_m is the maximum electric field and is given as:

Table 1
Donor concentration N_D, built-in voltage V_{bi}, fermi energy E_f, effective density of states in the Si valance band N_C, depletion layer width W_D, interface states N_{SS}, maximum electric field E_m, image force barrier lowering $\Delta\varphi_b$ parameters obtained from *C-V* measurements.

Temperature (K)	N_D(cm^{-3})	V_{bi} (eV)	E_f (eV)	N_C(cm^{-3})	W_D(cm)	N_{SS}(eV^{-1}cm^{-2})	E_m(Vm^{-1})	$\Delta\varphi_b$(eV)
300	2.54×10^{17}	1.72	0.26	1.02×10^{13}	1.67×10^{-7}	1.33×10^{12}	9553.40	1.08×10^{-3}
280	2.28×10^{17}	1.68	0.24	9.21×10^{12}	1.77×10^{-7}	1.11×10^{12}	8945.86	1.04×10^{-3}
260	2.10×10^{17}	1.66	0.23	8.24×10^{12}	1.84×10^{-7}	1.79×10^{12}	8529.53	1.02×10^{-3}
240	1.93×10^{17}	1.62	0.21	7.31×10^{12}	1.92×10^{-7}	1.87×10^{12}	8077.63	9.92×10^{-4}
220	1.74×10^{17}	1.59	0.19	6.42×10^{12}	2.02×10^{-7}	2.81×10^{12}	7609.89	9.63×10^{-4}
200	1.64×10^{17}	1.57	0.18	5.56×10^{12}	2.08×10^{-7}	3.80×10^{12}	7328.24	9.45×10^{-4}
180	1.58×10^{17}	1.54	0.16	4.75×10^{12}	2.12×10^{-7}	4.52×10^{12}	7116.41	9.31×10^{-4}
160	1.49×10^{17}	1.50	0.15	3.98×10^{12}	2.18×10^{-7}	7.17×10^{12}	6842.07	9.13×10^{-4}
140	1.39×10^{17}	1.46	0.13	3.26×10^{12}	2.26×10^{-7}	1.01×10^{13}	6513.32	8.91×10^{-4}
120	1.35×10^{17}	1.44	0.11	2.58×10^{12}	2.29×10^{-7}	1.58×10^{13}	6374.52	8.82×10^{-4}
100	1.27×10^{17}	1.39	0.10	1.97×10^{12}	2.37×10^{-7}	2.45×10^{13}	6053.12	8.59×10^{-4}
80	1.22×10^{17}	1.35	0.08	1.41×10^{12}	2.41×10^{-7}	3.97×10^{13}	5869.13	8.46×10^{-4}

$$E_m = \left(\frac{2qV_0N_D}{4\pi\varepsilon_S\varepsilon_0} \right)^{1/2} \tag{15}$$

By substituting the values of V_{bi}, E_f and $\Delta\varphi_b$ in equation (12), $\varphi_{b(C-V)}$ can be calculated at different temperature. The depletion layer width can be calculated by using the relation [57].

$$W_D = \sqrt{\frac{2\varepsilon_S(V_{bi} + V)}{qN_DA^2}} \tag{16}$$

The expression for the density of interface states in equilibrium with semiconductor as deduced by the Card and Rhoderick [59] is reduced as

$$N_{SS} = \frac{1}{q}\left[\frac{\varepsilon_i}{\delta}(n(V) - 1) - \frac{\varepsilon_s}{W_D} \right] \tag{17}$$

where ε_i is the permittivity and δ is the thickness of the interfacial layer.

The various temperature dependent parameters determined from the *C-V* measurements for the heterostructure Ni/*n*-TiO$_2$/*p*-Si/Al are summarized in Table 1. From Table 1, it was found that the values donor concentration, built-in voltage, fermi energy, effective density of states in the Si valance band, maximum electric field, image force barrier lowering increase with the increase in temperature while the depletion layer width and interface states decrease with increasing temperature.

The values of barrier heights determined from the *C-V* as well as from *I-V* data along with built-in voltage are shown in Fig. 13. The value of barrier height obtained from the *C-V* data is larger than the obtained from the *I-V* data. This may be due to in-homogeneities such as non-uniformity of interfacial layer, thickness and the distribution of interfacial charges at metal-semiconductor interface [54,61,62]. The *C-V* technique include an average value of barrier heights of patches available in the contact. Moreover, the effective barrier height obtained from the *I-V* measurements is sensitive to barrier lowering effect due to the interface
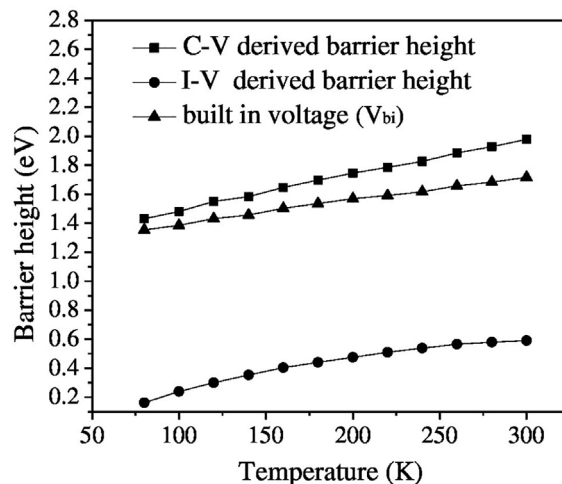

Fig. 13. Variation of barrier height derived from the current-voltage, capacitance-voltage measurements and built-in voltage with temperature for the heterojunction diode at 1 MHz frequency.

states effect. Other than this, the determination of barrier height from *I-V* characteristics is reliable if one can be confident that the current is determined by thermionic emission theory and this can be possible only if forward portion of the characteristics is straight line with low value of ideality factor [63,64].

4. Conclusions

The PLD deposited TiO_2 thin films on *p*-Si (100) wafer in oxygen-controlled environment exhibit single rutile phase having (210) as preferred direction. The prepared thin films are of nanocrystalline nature with grain size 43.3 nm. The optical studies revealed that rutile TiO_2 exhibits sharp absorbance and possess optical band gap of 3.20 eV. Atomic force microscopy studies of the surface morphology reveal that the surface is reasonably smooth, homogeneous and the roughness is of the nanometer order. The electrical transport study of considered heterojunction shows good rectifying properties at 300 K and similar characteristics are observed down to 80 K temperature. The experimental evaluation of forward biased *I-V* results reveal that zero-biased barrier height increases while ideality factor decreases with increasing temperature. The non-linearity of activation energy plot is attributed to the temperature dependence of barrier height which clearly shows the deviation from pure thermionic emission mechanism. The non-ideal forward biased temperature dependent *I-V* characteristics can be satisfactorily explained by considering the interfacial barrier height in-homogeneities with Gaussian distributions of barrier heights which are responsible for the deviation of zero-bias barrier height and ideality factor at low temperatures. In the present study, Gaussian distribution of barrier heights describes the inhomogeneities with mean barrier height of 0.79eV and standard deviation 0.10 V. The value of Richardson constant A^{**} has been obtained as 1.5×10^5 $Am^{-2}K^{-2}$ from the modified activation energy plot which is comparable with the theoretical known value for *p*-type silicon. The *C-V* characteristics show significant dependence on frequency and temperature. The barrier height of Ni/*n*-TiO_2/*p*-Si/Al heterojunction diodes were also obtained from the *C-V* measurements. The increase in the slopes values of the Mott-Schottky plot from the *C-V* measurements was attributed to the presence of interface states effect. The donor concentration, built-in voltage, fermi energy, effective density of states in the Si valance band, interface states, maximum electric field, image force barrier lowering and depletion layer width are the temperature dependent parameters.

References

[1] D.R. Lide, Handbook of Chemistry and Physics, Boca Raton, CRC Press Inc., 1991.
[2] Z.S. Hosseini, M. Shasti, S.R. Sani, A. Mortezaali, Photo-detector diode based on thermally oxidized TiO_2 nanostructures/*p*-Si heterojunction, J. Appl. Phys. 119 (2016) 014503.
[3] S. Bengi, M.M. Bulbul, Electrical and dielectric properties of Al/HfO_2/*p*-Si MOS device at high temperatures, Curr. Appl. Phys. 13 (2013) 1819–1825.
[4] I. Dokme, S. Altindal, Comparative analysis of temperature-dependent electrical and dielectric properties of an $Al-TiW-Pd_2Si/n$-Si Schottky device at two frequencies, IEEE Trans. Electron. Dev. 58 (2011) 4042–4048.
[5] A. Kaya, O. Vural, H. Tecimer, S. Demirezen, S. Altindal, Frequency and voltage dependence of dielectric properties and electric modulus in Au/PVC + TCNQ/*p*-Si structure at room temperature, Curr. Appl. Phys. 14 (2014) 322–330.
[6] H. Dogan, H. Korkut, N. Yildirim, A. Turut, Prediction of lateral barrier height in identically prepared Ni/*n*-type GaAs Schottky barrier diodes, Appl. Surf. Sci. 253 (2007) 7467–7470.
[7] G. Guler, O. Gullu, O.F. Bakkaloglu, A. Turut, Determination of lateral barrier height of identically prepared Ni/*n*-type Si Schottky barrier diodes by electro-deposition, Physica B 403 (2008) 2211–2214.
[8] A. Sariyildiz, O. Vural, M. Evecen, S. Altindal, Single Gaussian distribution of barrier height in Al/PS–ZnPc/*p*-Si type Schottky barrier diode in temperature range of 120–320 K, J. Mater. Sci. Mater. Electron. 25 (2014) 4391–4397.
[9] M. Biber, Low-temperature current–voltage characteristics of MIS Cu/*n*-GaAs and inhomogeneous Cu/n-GaAs Schottky diodes, Physica B 325 (2003) 138–148.
[10] O. Pakma, N. Serin, T. Serin, S. Altindal, The double Gaussian distribution of barrier heights in Al/TiO_2/*p*-Si (metal-insulator-semiconductor) structures at low temperatures, J. Appl. Phys. 104 (2008) 014501.
[11] M. Duta, S. Simeonov, V. Teodorescu, L. Predoana, S. Preda, M. Nicolescu, A. Marin, D. Spasov, M. Gartner, M. Zaharescu, A. Szekeres, Structural and electrical properties of Nb doped TiO_2 films prepared by the sol-gel layer-by-layer technique, Mater. Res. Bull. 74 (2016) 15–20.
[12] E. Gyorgy, A. Perez del Pino, G. Sauthier, A. Figueras, F. Alsina, J. Pascual, Structural, morphological and local electric properties of TiO_2 thin films grown by pulsed laser deposition, J. Phys. D Appl. Phys. 40 (2007) 5246–5251.
[13] J.H. Kim, S. Lee, H.S. Im, The effect of target density and its morphology on TiO_2 thin films grown on Si (l00) by PLD, Appl. Surf. Sci. 151 (1999) 6–16.
[14] O. Pakma, N. Serin, T. Serin, S. Altindal, The effects of preparation temperature on the main electrical parameters of Al/TiO_2/*p*-Si (MIS) structures by using sol–gel method, J. Sol. Gel Sci. Technol. 50 (2009) 28–34.
[15] B. Karunagaran, K. Kim, D. Mangalaraj, J. Yi, S. Velumani, Structural, optical and Raman scattering studies on DC magnetron sputtered titanium dioxide thin films, Sol. Energy Mater. Sol. Cell. 88 (2005) 199–208.
[16] B.S. Jeong, D.P. Norton, J.D. Budai, Conductivity in transparent anatase TiO_2 films epitaxially grown by reactive sputtering deposition, Solid State Electron. 47 (2003) 2275–2278.
[17] P. Zeman, S. Takabayashi, Effect of total and oxygen partial pressures on structure of photocatalytic TiO_2 films sputtered on unheated substrate, Surf. Coating. Technol. 153 (2002) 93–99.
[18] K. Okimura, Low temperature growth of rutile TiO_2 films in modified rf magnetron sputtering, Surf. Coating. Technol. 135 (2001) 286–290.
[19] D. Mardare, G.I. Rusu, Structural and electrical properties of TiO_2 rf sputtered thin films, Mater. Sci. Eng. B 75 (2000) 68–71.
[20] Y. Ishikawa, Y. Matsumoto, Electrodeposition of TiO_2 photocatalyst into nano-pores of hard alumite, Electrochim. Acta 46 (2001) 2819–2824.
[21] T. Tunc, I. Uslu, I. Dokme, S. Altindal, H. Uslu, Frequency and temperature dependence of dielectric properties of Au/polyvinyl alcohol (Co, Ni-doped)/*n*-Si Schottky diodes, Int. J. Polym. Mater. 59 (2010) 739–756.
[22] S. Alialy, S. Altindal, E.E. Tanrikulu, D.E. Yildiz, Analysis of temperature dependent current-conduction mechanisms in Au/TiO_2/*n*-4H-SiC (metal/insulator/semiconductor) type Schottky barrier diodes, J. Appl. Phys. 116 (2014) 083709.
[23] F. Hossein-Babaei, M.M. Lajvardi, N. Alaei-Sheini, The energy barrier at noble metal/TiO_2 junctions, Appl. Phys. Lett. 106 (2015) 083503.
[24] M.A. Khan, Y. Kang, Synthesis and electrochemical analysis of a nanostructured spindle shaped TiO_2, Mater. Lett. 156 (2015) 209–213.
[25] Y.S. Asar, T. Asar, S. Altindal, S. Ozcelik, Investigation of dielectric relaxation and ac electrical conductivity using impedance spectroscopy method in (AuZn)/TiO_2/*p*-GaAs(110) Schottky barrier diodes, J. Alloy. Comp. 628 (2015) 442–449.
[26] N.M. Mohamed, M. Khatani, N.H. Hamid, A.Z. Sahmer, S.N.A. Zaine, Performance analysis of dye solar cell with additional TiO_2 layer under different light Intensities, Mater. Sci. Semicond. Process. 38 (2015) 381–386.
[27] B. Tsui, J. Cheng, L. Lee, C. Lee, M. Tsai, Schottky barrier height modification of metal/4H-SiC contact using ultra-thin TiO_2 insertion method, Jpn. J. Appl. Phys.

53 (2014) 04EP10.

[28] B. Gao, T.M. Lim, D.P. Subagio, T.T. Lim, Zr-doped TiO_2 for enhanced photocatalytic degradation of bisphenol A, Appl. Catal., A 375 (2010) 107–115.

[29] B.O. Regan, M. Gratzel, A low-cost, high-efficiency solar cell based on dye-sensitized colloidal TiO_2 films, Nature 353 (1991) 737–740.

[30] A. Umar, M.S. Akhtar, R.I. Badran, M. Abaker, S.H. Kim, A. Al-Hajry, S. Baskoutas, Electrical properties of solution processed *p*-SnS nanosheets/*n*-TiO_2 heterojunction assembly, Appl. Phys. Lett. 103 (2013) 101602.

[31] A.M. Selman, Z. Hassan, Highly sensitive fast-response *UV* photodiode fabricated from rutile TiO_2 nanorod array on silicon substrate, Sens. Actuators: Physica 221 (2015) 15–21.

[32] J. Yu, S.J. Ippolito, W. Wlodarski, M. Strano, K. Kalantar-zadeh, Nanorod based Schottky contact gas sensors in reversed bias condition, Nanotechnology 21 (2010) 265502.

[33] B. Kinaci, T. Asar, Y. Ozen, S. Ozcelik, The analysis of Au/TiO_2/*n*-Si Schottky barrier diode at high temperatures using *I-V* characteristics, Optoelectronics and Advanced Materials-Rapid communications 5 (2011) 434.

[34] E. Hernandez-Rodriguez, A. Marquez-Herrera, E. Zaleta-Alejandre, M. Melendez-Lira, W. de la Cruz, M. Zapata-Torres, Effect of electrode type in the resistive switching behaviour of TiO_2 thin films, J. Phys. D Appl. Phys. 46 (2013) 045103.

[35] W.Y. Park, G.H. Kim, J.Y. Seok, K.M. Kim, S.J. Song, M.H. Lee, C.S. Hwang, A Pt/TiO_2/Ti Schottky-type selection diode for alleviating the sneak current in resistance switching memory arrays, Nanotecnology 21 (2010) 195201.

[36] T. Ivanova, A. Harizanova, T. Koutzarova, B. Vertruyen, Optical and structural characterization of TiO_2 films doped with silver nanoparticles obtained by sol–gel method, Opt. Mater. 36 (2013) 207–213.

[37] M.H. Suhail, G.M. Rao, S. Mohan, Dc reactive magnetron sputtering of titanium-structural and optical characterization of TiO_2 films, J. Appl. Phys. 71 (1992) 1421.

[38] B.J. Choi, D.S. Jeong, S.K. Kim, C. Rohde, S. Choi, J.H. Oh, H.J. Kim, C.S. Hwang, K. Szot, R. Waser, B. Reichenberg, S. Tiedke, Resistive switching mechanism ofTiO2thin films grown by atomic-layer deposition, J. Appl. Phys. 98 (2005) 033715.

[39] P. Kuppusami, V.S. Raghunathan, Status of pulsed laser deposition: challenges and opportunities, Surf. Eng. 22 (2006) 81–83.

[40] R. Kumar, S. Chand, Fabrication and Electrical Characterization of nickel/p-Si Schottky diode at low temperature, Solid State Sci. 58 (2016) 115–121.

[41] S. Chand, J. Kumar, Current transport in Pd_2Si/*n*-Si(100) Schottky barrier diodes at low temperatures, Appl. Phys. A 63 (1996) 171.

[42] M.M. Lajvardi, M. Jahangiri, Ni/TiO_2 ultraviolet detector, Mater. Sci. Eng. 108 (2016) 012031.

[43] B.D. Cullity, Elements of X-ray Diffraction, 2nd ed., Addison-Wesley Reading, MA, 1978.

[44] M.C. Sekhar, P. Kondaiah, G.M. Rao, S.V.J. Chandra, S. Uthanna, Post-deposition annealing influenced structural and electrical properties of Al/TiO_2/Si gate capacitors, Superlattice. Microst. 62 (2013) 68–80.

[45] W. Chiappim, G.E. Testoni, R.S. Moraes, R.S. Pessoa, J.C. Sagas, F.D. Origo, L. Vieira, H.S. Maciel, Structural, morphological, and optical properties of TiO2 thin films grown by atomic layer deposition on fluorine doped tin oxide conductive glass, Vacuum 123 (2016) 91–102.

[46] R. Weingärtner, J.A. Guerra Torres, O. Erlenbach, G. Gálvez de la Puente, F. De Zela, A. Winnacker, Bandgap engineering of the amorphous wide bandgap semiconductor $(SiC)_{1-x}(AlN)_x$ doped with terbium and its optical emission properties, Mater. Sci. Eng. B 174 (2010) 114–118.

[47] J. Tauc, F. Abeles, F. Abeles (Ed.), Optical properties of solids, 1972 North-Holland Amsterdam.

[48] M. Alijani, B.K. Kaleji, Optical and structural properties of TiO_2 nanopowders with Ce/Sn doping at various calcination temperature and time, Opt. Quant. Electron. 49 (34) (2017) 1–16.

[49] F.A. Grant, Properties of rutile (titanium dioxide), Rev. Mod. Phys. 31 (1959) 646–674.

[50] G. Rawat, D. Somvanshi, H. Kumar, Y. Kumar, C. Kumar, S. Jit, Ultraviolet detection properties of *p*-Si/*n*-TiO_2 heterojunction photodiodes grown by electron-beam evaporation and sol–gel methods: a comparative study, IEEE Trans. Nanotechnol. 15 (2016) 193–200.

[51] J.J. Huang, C.W. Kuo, W.C. Chang, T.H. Hou, Transition of stable rectification to resistive-switching in Ti/TiO_2/Pt oxide diode, Appl. Phys. Lett. 96 (2010) 262901.

[52] S. Chand, J. Kumar, On the existence of a distribution of barrier heights in Pd_2Si/Si Schottky diodes, J. Appl. Phys. 80 (1996) 288–294.

[53] J.H. Werner, H.H. Guttler, Barrier inhomogeneities at Schottky contacts, J. Appl. Phys. 69 (1991) 1522–1533.

[54] Y.P. Song, R.L.V. Meirhaeghe, W.H. Laflere, F. Cardon, On the difference in apparent barrier height as obtained from capacitance-voltage and current-voltage-temperature measurements on Al/*p*-InP Schottky barriers, Solid State Electron. 29 (1986) 633–638.

[55] V.V. Brus, A.K.K. Kyaw, P.D. Maryanchuk, J. Zhang, Quantifying interface states and bulk defects in high-efficiency solution-processed small-molecule solar cells by impedance and capacitance characteristics, Prog. Photovoltaics Res. Appl. 23 (2015) 2586.

[56] S. Chand, R. Kumar, Electrical characterization of Ni/*n*-ZnO/*p*-Si/Al heterostructure fabricated by pulsed laser deposition technique, J. Alloy and compound 613 (2014) 395–400.

[57] M. Sharma, S.K. Tripathy, Study of barrier inhomogeneities in I–V-T and C-V-T characteristics of Al/Al_2O_3/PVA:*n*-ZnSe metal–oxide–semiconductor diode, J. Appl. Phys. 112 (2012) 024521.

[58] O. Gullu, S. Aydogan, A. Turut, High barrier Schottky diode with organic interlayer, Solid State Commun. 152 (2012) 381–385.

[59] O. Pakma, N. Serin, T. Serin, S. Altindal, On the energy distribution profile of interface states obtained by taking into account of series resistance in Al/TiO_2/p–Si (MIS) structures, Physica B 406 (2011) 771–776.

[60] E.E. Tanrikulu, D.E. Yildiz, A. Gunen, S. Altindal, Frequency and voltage dependence of electric and dielectric properties of Au/TiO_2/n-4H-SiC (metal-insulator-semiconductor) type Schottky barrier diodes, Phys. Scripta 90 (2015) 095801.

[61] K.M. Kim, B.J. Choi, M.H. Lee, G.H. Kim, S.J. Song, J.Y. Seok, J.H. Yoon, S. Han, C.S. Hwang, A detailed understanding of the electronic bipolar resistance switching behavior in Pt/TiO_2/Pt structure, Nanotechnology 22 (2011) 254010.

[62] B. Akkal, Z. Benamara, B. Gruzza, L. Bideux, Characterization of interface states at Au/InSb/InP(100) Schottky barrier diodes as a function of frequency, Vacuum 57 (2000) 219–228.

[63] E.H. Rhoderick, R.H. Williams, Metal-semiconductor Contacts, Clarendon Press, Oxford, 1988.

[64] S. Altindal, S. Karadeniz, N. Tugluoglu, A. Tataroglu, The role of interface states and series resistance on the *I–V* and *C–V* characteristics in Al/SnO_2/*p*-Si Schottky diodes, Solid State Electron. 47 (2003) 1847–1854.